IEICE Proceeding Series

Nonlinear Rotor Response with Coupled Lateral and Torsional Motions

Nicholas Vlajic, Hamad Karki, Balakumar Balachandran

Vol. 2 pp. 22-25
Publication Date: 2014/03/18
Online ISSN: 2188-5079

Nonlinear Rotor Response with Coupled Lateral and Torsional Motions

Nicholas Vlajic†, Hamad Karki‡, and Balakumar Balachandran†

†Department of Mechanical Engineering, University of Maryland
College Park, MD 20742, USA
Email: vlajic@umd.edu, balab@umd.edu
‡Department of Mechanical Engineering, The Petroleum Institute
Abu Dhabi, UAE
Email: hkarki@pi.ac.ae

Abstract—In previous work of the authors, experimental response data for a slender rotor system with gyroscopically coupled lateral and torsional motions were presented along with a computational model that was used to predict and explain phenomena observed in the experiments. Here, the authors expand upon this work, develop a reduced-order system to study the system torsion dynamics in the presence of continuous rotor-stator contact, and carry out analysis to develop insights into the origins of the frequency-response components observed in the experiments and simulations.

1. Introduction

Torsional and lateral motions of a rotor system can be strongly coupled when the rotating shaft becomes slender and/or with the addition of discrete mass elements along the shaft. Furthermore, if the mass addition is not at the mid-span of the shaft, the lateral motions can also be coupled through gyroscopic terms [1]. In the authors' previous work, they investigated the torsion response of a slender shaft with gyroscopic coupling while the rotor was in continuous contact with a stator. Torsional motions were further excited by friction forces that arise due to contact with the stator. In addition to the experimental data presented in reference [2], a distributed parameter model was developed and used to understand the experimentally observed dynamics. In the current effort, the authors further examine these equations in a similar manner to their approach method outlined in study [3]. This is done in order to develop a single degree-of-freedom, reduced-order equation for focusing on the torsional motions while the rotor is in continuous contact with the stator of this system.

2. Summary of Previous Work

2.1. Experimental Arrangement and Results

A photograph of the experimental arrangement is shown in Figure 1. A DC motor turns a stiff drive shaft and self-centering three jaw chuck. The chuck holds a slender aluminum 6061 string that is vertically suspended and has a rotor secured to its bottom end. This rotor is enclosed within a circular stator with an initial gap clearance δ. A slip ring is fitted onto the stiff shaft, so that sensors may be secured to the rotating structure. To collect the particular experimental data shown here, strain gages are placed in a rosette configuration in order to get a measure of the torsional motions.

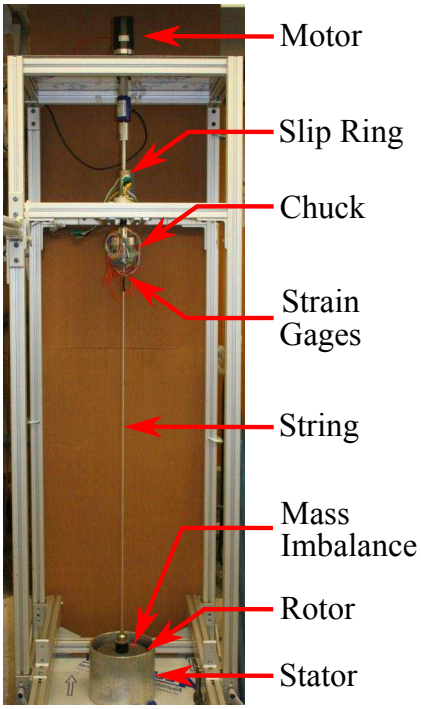

Figure 1: Experimental apparatus used to study dynamics of rotor-stator systems, which was originally presented in reference [2].

For certain initial conditions and driving speeds, the rotor remains in continuous contact with the stator while the rotor whirls at a constant rate. The Fourier transforms of the torsion strain response associated with forward whirling (rotor whirl motions in the same direction as the motor rotation) are presented in Figure 2 (a), while Fourier transforms of the torsional strain response associated with backward whirling (rotor whirl motions in the opposite direction of motor rotation) are provided in Figure 2 (b). It has been confirmed both experimentally and nu-

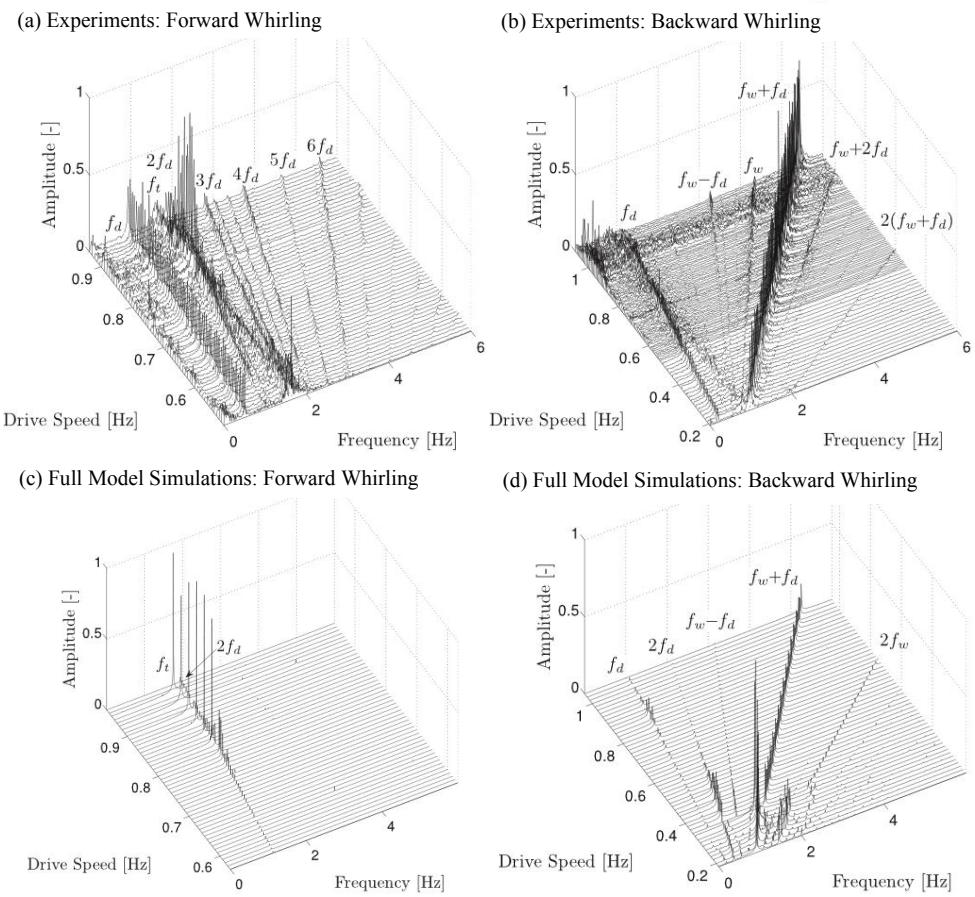

Figure 2: Summary of the results presented in study [2]. (a) Experimentally obtained torsion strain spectra during forward whirling. (b) Experimentally obtained torsion strain spectra during backward whirling. (c) Simulation predictions of the torsion response spectra for forward whirling motions. (d) Simulation predictions of the torsion response spectra for backward whirling motions.

merically that during forward whirling, the rotor whirl frequency is approximately equal to the motor drive frequency ($\omega_{for} \approx \Omega$), where Ω is the drive speed in rad/s and ω_{for} denotes the forward whirling frequency in rad/s. Throughout this work, ω and Ω, are angular frequencies that have units of rad/s, while frequency quantities denoted with f have units of Hz. It has been verified that during backward whirling, the whirl frequency of the rotor may be expressed in terms of the system parameters ($\omega_{back} \approx -\frac{R}{\delta}\Omega$). From the experimental spectra shown in Figures 2 (a) and (b), the prominent frequency components during forward whirling are at the first torsion natural frequency (f_t), the drive frequency (f_d), and twice the drive frequency ($2f_d$). During backward whirling, components at the drive frequency (f_d) and the whirl frequency plus the drive frequency ($f_w + f_d$), dominate the system response. It is noted that the f_d component in the forward whirling response arises due to a small eccentricity in the chuck, and this has not been captured in simulations.

2.2. Model Predictions and Comparisons with Experiments

After constructing energy expressions for a shaft modeled as a spatially continuous structure and the rotor modeled as a discrete mass at the boundary, a set of three nonlinear partial differential equations and ten boundary conditions were derived. A Galerkin projection procedure, with a single mode approximation for each equation in bending and torsion, was used to cast the system of partial differential equations into the following set of ordinary differential equations

$$a_1\ddot{V} + a_2\dot{V} + a_3\Omega\dot{W} + a_4 V + a_5(\dot{\Theta}\dot{W} + \ddot{\Theta}W) - me\phi_\theta\phi_v\ddot{\Theta}\sin(\beta)\Big|_{x=L} - me\phi_v\dot{\beta}^2\cos(\beta)\Big|_{x=L} = \phi_v F_v\Big|_{x=L} \quad (1)$$

$$b_1\ddot{W} + b_2\dot{W} + \Omega b_3\dot{V} + b_4 W + b_5\dot{\Theta}\dot{V} + me\phi_w\phi_\theta\ddot{\Theta}\cos(\beta)\Big|_{x=L} - me\phi_w\dot{\beta}^2\sin(\beta)\Big|_{x=L} = \phi_w F_w\Big|_{x=L} \quad (2)$$

$$c_1\ddot{\Theta} + c_2\dot{\Theta} + c_3\Theta + c_4(\ddot{V}W + \dot{V}\dot{W}) + me\ddot{W}\phi_w\phi_\theta\cos(\beta)\Big|_{x=L} - me\ddot{V}\phi_v\phi_\theta\sin(\beta)\Big|_{x=L} = \phi_\theta F_{tan}R\Big|_{x=L} \quad (3)$$

where

$$\beta = \phi_\theta \Theta + \Omega t$$

In equations (1) - (3), $V \equiv V(t)$, $W \equiv W(t)$, and $\Theta \equiv \Theta(t)$ are the temporal amplitudes associated with the shape functions $\phi_v \equiv \phi_v(x)$, $\phi_w \equiv \phi_w(x)$, and $\phi_\theta \equiv \phi_\theta(x)$, respectively. A more detailed description of the Galerkin procedure used to obtain these equations, as well as the explicit forms of the coefficients of equations (1) - (3) may be found in the authors' work [2]. The external forces in equations (1)-(3) are determined as follows. When in contact with the stator, the rotor is subject to a normal force, which is given by

$$F_{norm} = \begin{cases} 0 & \text{for } \Gamma \leq \delta \\ K_c(\Gamma - \delta) & \text{for } \Gamma > \delta \end{cases} \tag{4}$$

where

$$\Gamma = \sqrt{w(L,t)^2 + v(L,t)^2}$$

Additionally, a tangential force, which is proportional to the normal force, is generated as

$$F_{tan} = \mu \cdot F_{norm} \tag{5}$$

where the friction coefficient

$$\mu = -\frac{2}{\pi}\arctan(\epsilon_f v_{rel})\left[\frac{\mu_s - \mu_d}{1 + \delta_f |v_{rel}|} + \mu_d\right] \tag{6}$$

This choice of friction model captures the different friction magnitudes between static friction and dynamic friction. Here, the slope of the frictional force is negative near $v_{rel} = 0$, but becomes a constant away from 0. The authors have generated Figures 2 (c) and (d) by numerically integrating equations (1)-(3).

3. Reduction of Equations of Motion

Following a procedure that was originally outlined by the authors in [3], the system of equations given by equations (1)-(3) are reduced to a single nonlinear differential equation which is meant for studying the torsional motions during steady-state whirl. For constant whirl frequencies, the lateral motions of the rotor at $x = L$ may be prescribed as

$$\begin{aligned} v(L,t) &= (\delta + \delta_p)\cos(\omega t + \phi_o) \approx \delta \cos \omega t \\ w(L,t) &= (\delta + \delta_p)\sin(\omega t + \phi_o) \approx \delta \sin \omega t \end{aligned} \tag{7}$$

where the penetration depth δ_p of the rotor into the stator is approximately zero. Considering small torsional deformations, the respective Taylor series expansions are carried out with the trigonometric terms in Θ. After substituting these expansions into the governing equations, the following reduced-order equation is obtained to focus on the torsion dynamics:

$$c_1\ddot{\Theta} + c_2\dot{\Theta} + \left[c_3 + \phi_\theta(L) me\delta\omega^2 \cos((\omega - \Omega)t)\right]\Theta = c_4\omega^2 \sin(2\omega t) + \phi_\theta(L) me\delta\omega^2 \sin((\omega - \Omega)t) + \phi_\theta(L) F_{tan} R \tag{8}$$

Through the earlier imposed assumptions $\delta_p \approx 0$, and using equation (4), the normal force is zero. However, assuming the stator to be much stiffer than the rotor, the normal force may be found in terms of the reaction force as the rotor whirls in contact with the stator. This approximate form is taken to be

$$F_{norm} \approx M\delta\omega^2 - K_{eq}\delta \tag{9}$$

where it has been assumed that $\delta(M + m) \gg me$ and K_{eq} is the equivalent stiffness of shaft. This equation is given consideration in the remaining sections for both forward and backward whirling.

4. Forward Whirling

As previously mentioned, in the special case of forward whirling $\omega \approx \Omega$, equation (8) can be written as

$$c_1\ddot{\Theta} + c_2\dot{\Theta} + \left[c_3 + \phi_\theta(L) me\delta\omega^2\right]\Theta = c_4\omega^2 \sin(2\omega t) - \phi_\theta(L) F_{tan} R \tag{10}$$

Equation (10) has interesting features which are explained next. As discussed in study [3], equation (10) has a centrifugal stiffening term. However, due to the low drive speeds in the given experiment, this effect is small and unmeasurable. In other experiments at high drive speeds, researchers have observed a stiffening effect during steady whirl with constant stator contact [4]. The reduced-order equation also has an external forcing frequency of $2\Omega = 2\omega$, which originates solely from the gyroscopic coupling terms in equation (1)-(3). In the absence of friction, $F_{tan} = 0$, equation (10) takes the form of a linear oscillator with harmonic forcing, associated with which a resonance will occur if $2\Omega \approx \omega_t = \sqrt{\frac{c_3 + \phi_\theta(L) me\delta\omega^2}{c_1}} \approx \sqrt{\frac{c_3}{c_1}}$. This resonance behavior is apparent in both the experimental results shown in Figure 2 and in the results obtained from simulations of the full model (equations (1)-(3)) shown in Figure 2, as well as in the numerical results for the reduced-order model (equation (10)) provided in Figure 3(a). It is noted that near resonance, the original assumption of small angular deformations breaks down and equation (10) is no longer a reasonable approximation for the system dynamics in that region. Further, even in the absence of forcing originating from gyroscopic coupling (such as a planar rotor, for instance), one can still obtain limit-cycle motions from the form of equation (10), as was found in the authors' previous work [3]. Finally, a component at the torsion damped natural frequency is observed in the experiments shown in Figure 2(a), where the first torsion damped natural frequency is approximately equal to the undamped torsion frequency due to the light structural damping of the system. The response component at the first torsion natural frequency is not apparent in the simulations as the static coefficient of friction value was selected to be small. The response amplitude at this natural frequency is expected to be more prominent for other friction parameter values.

5. Backward Whirling

During backward whirling, the whirl speed of the lateral vibrations is approximately $\omega \approx -\frac{R}{\delta}\Omega$, and equation (8) can be rewritten as

$$c_1\ddot{\Theta} + c_2\dot{\Theta} + \left[c_3 + \phi_\theta(L)me\delta\omega^2\cos(\alpha t)\right]\Theta = c_4\omega^2\sin(2\omega t) - \phi_\theta(L)me\delta\omega^2\sin(\alpha t) + \phi_\theta(L)F_{tan}R \quad (11)$$

where

$$\alpha = (\omega - \Omega) = -\Omega(1 + \frac{R}{\delta}) \quad (12)$$

The frequency α physically represents the whirl speed, less the drive speed. This excitation frequency plays a role in equation (11) through external and parametric excitation terms. In both the experimental results shown in Figure 2 (b), simulations of the full model (equations (1)-(3)) shown in Figure 2 (d), and simulation results of the reduced-order model (equation (11)) provided in Figure 3 (b), the response component at the whirl frequency plus the drive frequency is the dominant component (note that Fourier transforms presented here do not distinguish between positive and negative frequencies). Additionally, the external forcing at frequency 2ω from the gyroscopic coupling is still present in equation (11) and in the simulation results shown in Figure 2 (d). However, this component is not discernibly large in the experimental results shown in Figure 2 (b), and in the numerical results obtained from the reduced-order equation and shown in Figure 3 (b).

6. Concluding Remarks

In previous work, the authors presented experimental data and numerical simulation results for a rotor-stator system, wherein the rotor experienced coupled lateral motions with large deformations. Here, the governing equations of motion were simplified under a given set of assumptions for continuous rotor-stator contact in order to develop a reduced-order system to focus on phenomena associated with experimentally observed torsional motions and numerical simulations of the full system of equations. It was determined that in both forward and backward whirling, an external excitation component arises due to gyroscopic coupling terms in the model. As a consequence, during forward whirling, even when driving the motor below the first torsion natural frequency, resonance behavior can occur provided $2\Omega = \omega_t$. Similarly, resonance behavior can occur in backward whirling if $\Omega(1 + \frac{R}{\delta}) = \omega_t$.

(a) Reduced-order: Backward Whirling

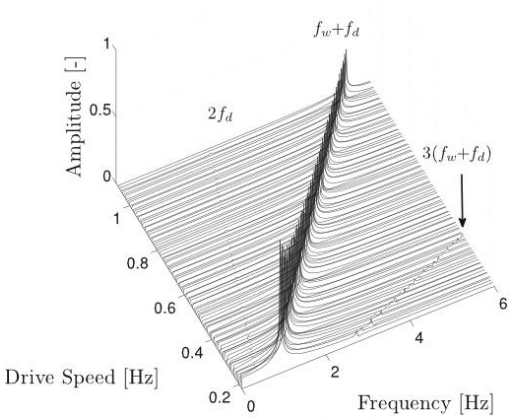

(b) Reduced-order: Forward Whirling

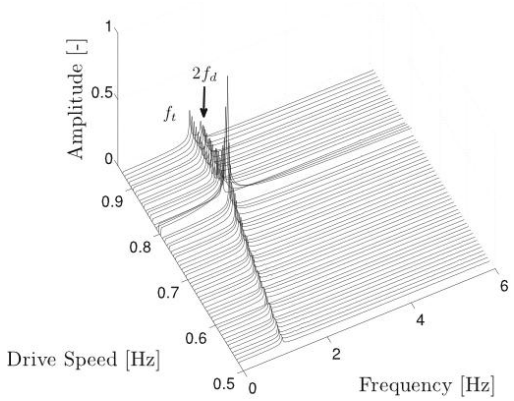

Figure 3: Fourier spectra of simulation time histories obtained from reduced-order equations. (a) Forward whirling results from equation (10). (b) Backward whirling results from equation (11).

References

[1] T. Yamamoto and Y. Ishida, "Linear and nonlinear rotordynamics," *John Wiley & Sons, Inc.*, 2001.

[2] N. Vlajic, X. Liu, H. Karki, and B. Balachandran, "Rotor torsion vibrations in the presence of continuous stator contact," *ASME IMECE*, Paper IMECE2012-89195, 2012.

[3] N. Vlajic, X. Liu, H. Karki, and B. Balachandran, "Torsion oscillations of a rotor with continuous stator contact," *Intl. J. of Mechanical Sciences*, to be submitted.

[4] H. Diangui, "Characteristics of torsional vibrations of rotor-to-stator rub in turbormachinery," *Tribology International*, vol.33, pp.75–79, 2000.